ACS Photonics

Letter

pubs.acs.org/journal/apchd5

Noble Metal Alloys for Plasmonics

Chen Gong[†,‡] and Marina S. Leite*[,†,‡]

[†]Department of Materials Science and Engineering and [‡]Institute for Research in Electronics and Applied Physics, University of Maryland, College Park, Maryland 20740, United States

Supporting Information

ABSTRACT: The fixed optical properties of noble metals currently limit their use in photonic devices that operate at optical frequencies. To achieve metals with tunable optical response, we present noble metal alloyed thin-films formed by the binary mixture of Ag, Au, and Cu. As the dielectric functions (ε) of the alloys cannot be modeled as the linear combination of the pure metals, we combined transmission and reflection measurements of the alloyed thin films with a B-spline model that takes into account the Kromers−Kronig relation and experimentally determined the dielectric functions. We found that in some cases a mixture can provide a material with higher surface plasmon polariton quality factor than the corresponding pure metals. We independently measured the surface plasmon polariton coupling angle for all alloys using the Kretschmann configuration and found excellent agreement between the two methods when determining ε. Our approach paves the way to implement metallic thin films and nanostructures with on-demand optical responses, overcoming the current limitation of the dielectric function of noble metals.

KEYWORDS: *plasmonics, dielectric function, gold, silver, copper, alloys*

If one had the option to arbitrarily modulate the dielectric function ($\varepsilon = \varepsilon_1 + i\varepsilon_2$) of metallic structures, this would enable unprecedented control of the plasmon resonances in nanostructures and the surface plasmon propagation in thin films.[1] This, in turn, would allow for the development of a new class of metallic materials with tunable optical response for the fabrication of optoelectronic devices with unique characteristics, such as metasurfaces[2−4] for tunable absorbers and optical filters, high-performance detectors,[5,6] and thin-film solar cells with enhanced performance,[7−9] among others. Therefore, ways to control the dielectric function of a material are potentially very useful. In situations where one wants to minimize the material light absorption, such as in low-loss metamaterials with rationally designed composition and geometry or photonic devices where surface plasmons propagate on the surface of the metal, a small imaginary part of the dielectric function (ε_2) is required. Conversely, when one desires to use a metal as a light absorbing layer, for example, in hot carrier devices and perfect absorbers,[10] a large value of ε_2 is essential.

Different classes of materials have been explored for plasmonics applications, including ceramics, intermetallics, semiconductors, and metals, depending on the desired wavelength range of operation.[11−13] One promising option to achieve low-loss plasmonic materials in the near-infrared (NIR) wavelength range is to realize transparent conducting oxides (TCO), such as doped zinc oxide (ZnO) and indium thin oxide (ITO).[11] Nitrides, such as TiN, are also a promising option for NIR applications.[14] These materials are radiation tolerant and can be epitaxially grown onto substrates with cubic symmetry,[12] which have the advantage of achieving ultrasmooth surfaces and thin-films without boundaries. Noble metals such as Ag and Au have been extensively explored due to their localized surface plasmon resonances (LSPR)[1] and surface plasmon polariton (SPP) waveguiding properties throughout the visible range.[1,15] However, despite all the research using noble metals, there are still considerable limitations related to their predetermined optical response.

One pathway to modulate the dielectric function of a metallic material is by alloying two metals.[16−22] Combinations of Ag, Au, and Cu represent an ideal model system to investigate how alloying can affect the optical properties of the mixed material due to their similar structural properties (cubic crystalline structure and lattice constants differ by less than 11%) and energy bands (comparable energy gaps for transitions between the *s*- and *d*-bands at similar symmetry points).[23] Nevertheless, ε of the alloyed metals cannot be approximated by the simple linear combination of the respective contribution from the individual metals because that would provide a physically nonrealistic optical response for the new material, including negative absorption.[18,24] Recently, it has been shown that the dielectric function of Ag−Au alloys can be predicted by using a multiparametric approach based on the Drude−Lorentz[25] model, taking into account the band structure of each pure metal separately.[26] Although ε for pure Ag, Au, and Cu has been extensively measured and calculated,[27−31] there is very little work investigating the interpolated behavior of ε as a function of a

Received: October 13, 2015
Published: February 24, 2016

DOI: 10.1021/acsphotonics.5b00586
ACS Photonics 2016, 3, 507−513

range of compositions for the respective binary noble metal alloys.

In this Letter, we present the tuning of the optical properties of thin-film noble metal mixtures by modification of their chemical composition, as a result of alloying. Thin films with a linear composition gradient formed by the binary mixture of Ag, Au, and Cu yielded alloys, an ideal model system to probe how the respective dielectric functions can be modulated by varying the content of each metal. Through the transmission and reflection measurements of the alloyed thin films and a B-spline model that takes into account the Kromers–Kronig relation, we experimentally determined the dielectric function of the noble metal alloys and found that, for the experimental conditions used here, in some cases a mixture of two metals can provide a material with higher SPP quality factor (Q_{SPP}) than the corresponding pure metals. We independently measured the SPP coupling angle for all alloys using the Kretschmann configuration and found excellent agreement between the two methods when determining ε. We provide a method for creating metallic thin films and nanostructures with tunable dielectric function, removing the predefined optical response constrain of pure noble metals.

Figure 1 shows the noble metal alloyed thin-film samples, formed by the binary linear combination of Ag, Au, and Cu, fabricated by cosputtering deposition (see Methods for the fabrication details). The evident color variation matches the composition gradient within the samples. In all cases, a linear gradient in composition was obtained (Figure S1 and Table S1), as desired. All samples were very smooth (roughness < 1.7 nm, as measured by AFM; see Figures S2 and S3)[32,33] and were composed of polycrystals, as determined by X-ray diffraction measurements (see Figure S4). All thin films were approximately 30 nm in thickness and, therefore, suitable for both transmission and SPP prism coupling measurements. Note that the hazy texture observed in the photograph of the samples is actually from the cleanroom wipes under the samples and not from the roughness of the samples itself.

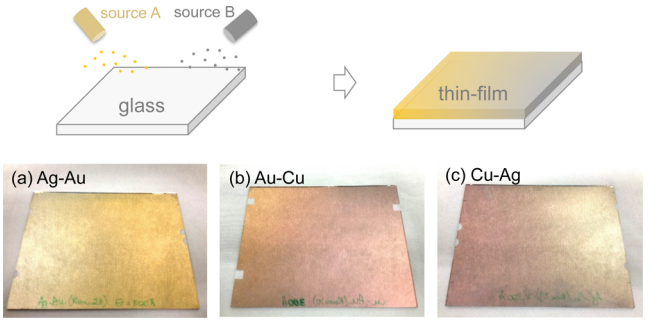

Figure 1. Thin-film noble metal alloys with on-demand optical response. (top) Schematic of the cosputtering process used to achieve alloyed thin-films with variable composition. (a–c) Photographs of three samples (nominal thickness = 30 nm in all cases) formed by binary combinations of Ag, Au, and Cu. Glass slides are 4 × 6 in^2.

Figure 2 displays the transmission spectra for all alloyed samples, acquired at equally spaced locations across each sample, corresponding to a well-defined composition of the alloyed films. As expected, the pure metals (Ag, Au, and Cu) showed respective transmission peaks at 324, 499, and 581 nm, attesting to the high quality of the films, despite the fact that the metals were sputtered at low deposition rates.[31] In all cases, the samples were measured immediately after being removed from the sputtering chamber, minimizing air exposure and consequent oxidation. As shown in Figure 2, the transmission measurements and are in very good agreement with the calculated transmission spectra. The $Ag_{0.5}Au_{0.5}$ alloy presents a broad peak at 454 nm, resulting from the contribution of both Ag and Au transmission signals, as shown in Figure 2a,b. In Figure 2c,d, all the Au_xCu_{1-x} alloys show one minor peak at ~350 nm and a major peak at 520–550 nm, resulting from both metals being present. The transmission spectra for the Cu_xAg_{1-x} sample (Figure 2e,f) present a continuous transition between the two pure metals, interpreted as a smooth change in relative intensity between the peaks of Cu and Ag. In particular, the region of the film corresponding to $Cu_{0.5}Ag_{0.5}$ shows a flat response over the 360 to 553 nm wavelength range. This behavior strongly indicates that the optical response of the alloys is not a result of the simple linear combination of the optical properties of the pure metals and requires a full investigation by an independent measurement technique, as will be discussed below.

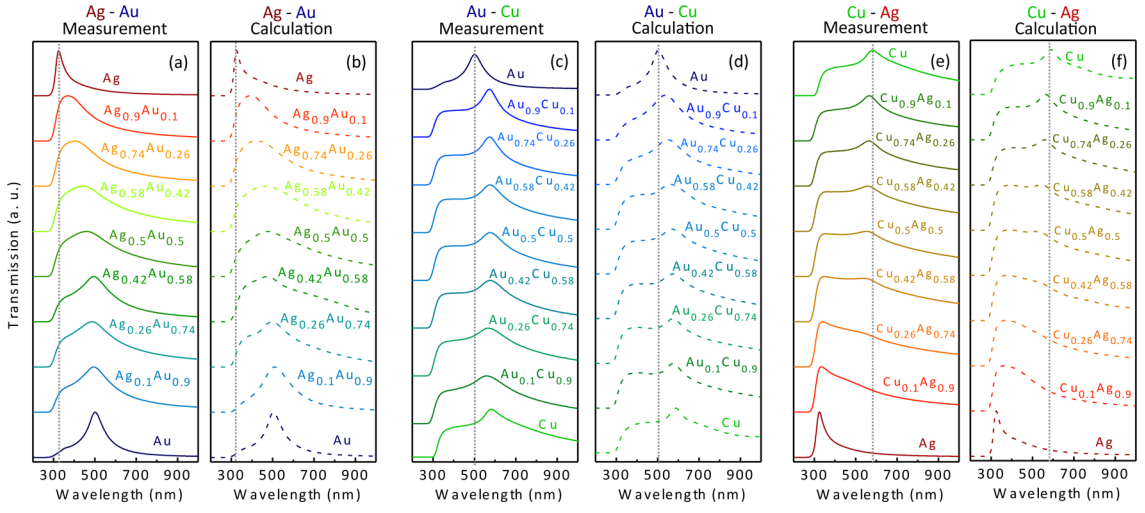

Figure 2. Transmission spectra of noble metal-alloyed thin films. Normalized transmission measurements and calculations for 30 nm thick (a,b) Ag–Au, (c,d) Au–Cu, and (e,f) Cu–Ag thin films on glass showing the dependence of the peak shifts with the film composition. The dashed lines are guides for the eyes, showing the wavelength shift from one pure metal to another.

DOI: 10.1021/acsphotonics.5b00586
ACS Photonics 2016, 3, 507–513

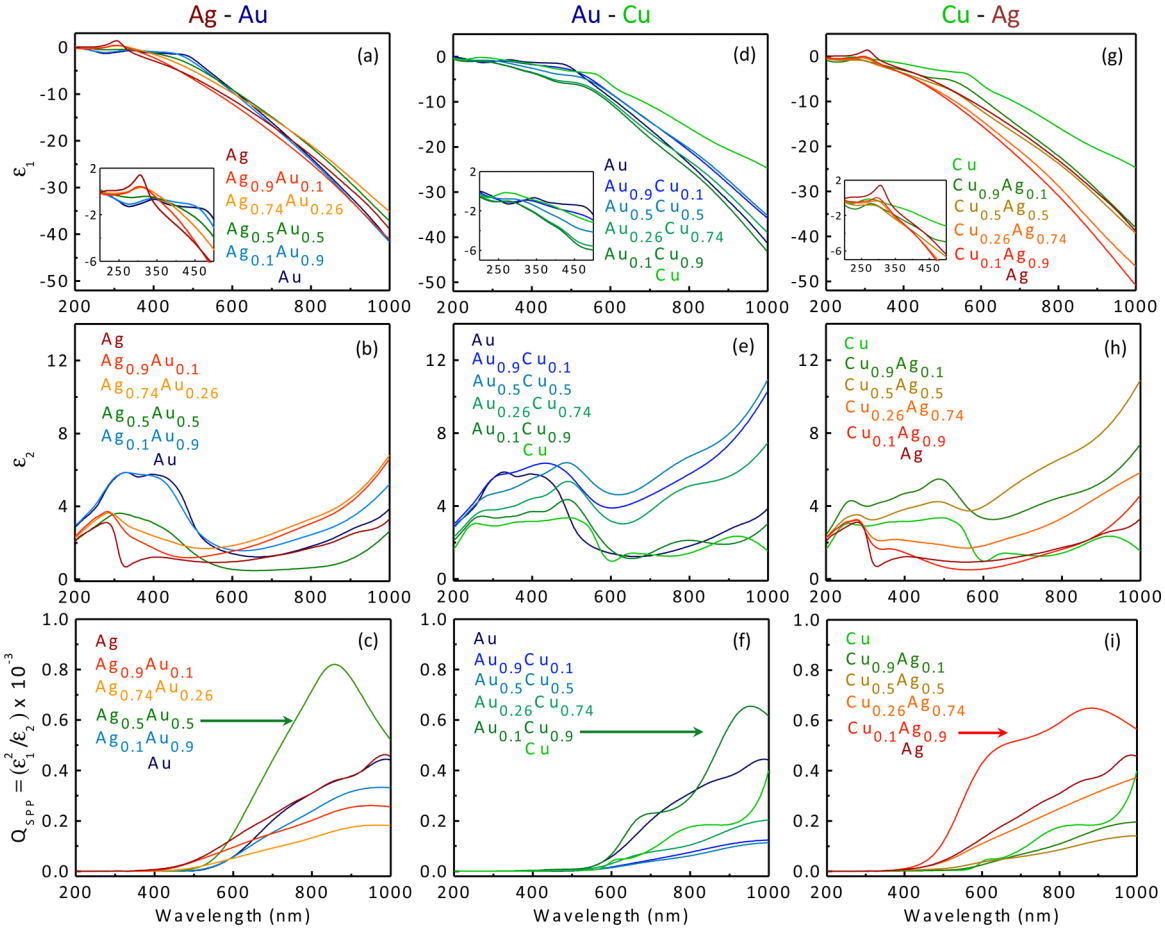

Figure 3. Measured dielectric function of noble metal alloyed thin films with variable composition. Real (ε_1) and imaginary (ε_2) parts of the dielectric function for metallic thin-films with variable composition: (a, b) Ag−Au, (d, e) Au−Cu, and (g, h) Cu−Ag thin films. Insets: zoom-in of ε_1 as a function of wavelength for the ultraviolet and visible regions of the spectrum. Surface plasmon polariton quality factor Q_{SPP} for (c) Ag−Au, (f) Au−Cu, and (i) Cu−Ag thin-film samples fabricated by sputtering, showing that metal alloyed thin films can outperform individual noble metals.

In order to probe how the optical response of the noble metal alloys changes as a function of material composition we measured the dielectric function ε of the thin films by ellipsometry, combining transmission and reflection measurements[34] (see Methods for the details concerning these measurements). To determine ε, we used a B-spline model[35] to describe the optical response of the alloyed thin films, where the Kromers−Kronig relation was enforced at all times and the film thickness was also a variable parameter (see Methods and SI). We verified the film thickness via cross-section TEM (see Figure S5) and found excellent agreement with the thickness value obtained by ellipsometry and the calculated optical response of the film. Figure 3 shows the measured real (ε_1) and imaginary (ε_2) parts of the dielectric function for all the noble alloyed thin films. The raw ellipsometry data for all samples (ψ and Δ as a function of wavelength) are presented in Figure S6. According to their phase diagram, Ag and Au form a solid solution over the whole concentration range,[17] with a nearly constant lattice parameter.[36] As a result, the degree of disorder of the Ag−Au mixture is also constant for the different compositions, leading to a similar mean free path of conduction electrons for all alloys. This explains why ε_1 and ε_2 for Ag−Au do not vary drastically from 400 to 900 nm (see Figure 3a,b). ε_2 has a minimum value equal to 0.5 at ∼700 nm, dominated by a disordered $Ag_{0.5}Au_{0.5}$ alloy.[26] The threshold of the interband transition, characterized by the sharp decrease of ε_2, changes from about 300 nm (pure Ag) to 500 nm (pure Au),[26] as shown in Figure 3b.

For the Au−Cu alloy system, multiphases can also be obtained over certain composition ranges, such as $Au_{0.25}Cu_{0.75}$, $Au_{0.5}Cu_{0.5}$, and $Au_{0.75}Cu_{0.25}$.[37] Here, the threshold of the interband transition shifted from 500 to 550 nm, from pure Au to pure Cu. From the spectrum of ε_2 (Figure 3e), the absence of peaks at 331 and 344 nm, corresponding to the ordered phase of $Au_{0.5}Cu_{0.5}$ and $Au_{0.26}Cu_{0.74}$, respectively, strongly indicates that these alloys form a disordered phase, as previously observed by Rivory.[22] Yet, De Silva recently reported that the overall effect of ordering on the dielectric function of Au−Cu is minor and can be easily masked by the scatter band resulting from variations of experimental measurements.[38] For instance, they observed that the Au−Cu porous thin-film was composed by small grains, and that the resulting high density of boundaries enhanced light scattering and therefore the absorption by the thin-film layer, causing an overall increase of ε_2. Conversely, they found that bulk Au−Cu was composed by large grains (almost free of defects and, thus, light scattering centers). Note that the experimental conditions of the film deposition can substantially affect the size of the grains constituting a film and the density of interfaces, which explains the different values of ε_2 reported by different groups. Postdeposition annealing treatments and the deposition rate are known for influencing the final structural characteristics and optical response of metal thin films.[31]

DOI: 10.1021/acsphotonics.5b00586
ACS Photonics 2016, 3, 507−513

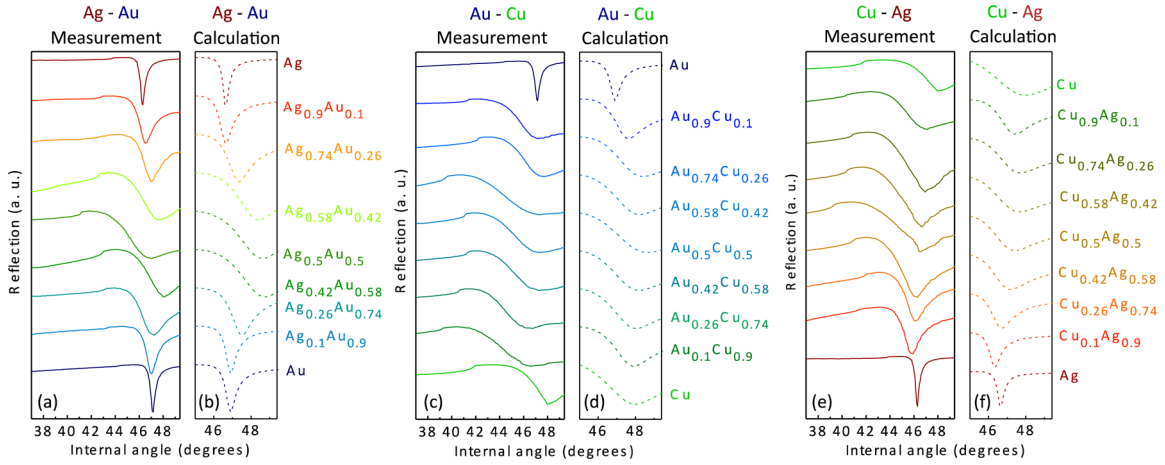

Figure 4. Surface plasmon polariton excitation in noble metal alloys. Measurements and calculations showing surface plasmon polariton excitation as a function of internal angle in a Kretschmann configuration for (a, b) Ag−Au, (c, d) Au−Cu, and (e, f) Cu−Ag thin films. Light source: 637 nm diode laser *p*-polarized with 3.6 mW.

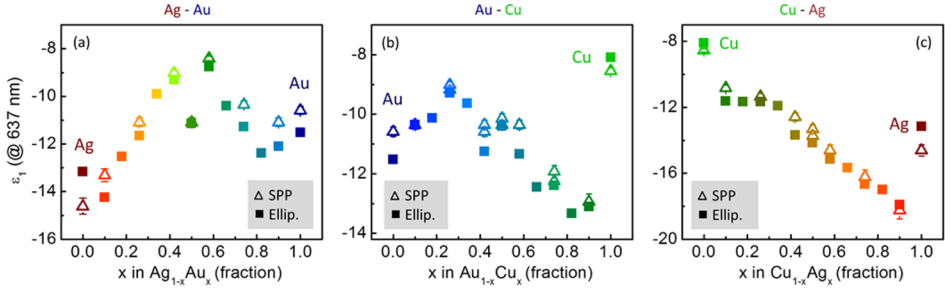

Figure 5. Optical response of metal-alloyed thin films. Real part of dielectric function ε_1 (at 637 nm) as a function of film composition, as determined from surface plasmon polariton excitation (SPP, open triangles) and ellipsometry (Ellip., solid squares) experiments for (a) Ag−Au, (b) Au−Cu, and (c) Cu−Ag thin films.

Conversely, the phase diagram of the Cu_xAg_{1-x} system has a broad miscibility gap for the whole composition range for room temperature deposition as Cu−Ag does not form a solid solution,[37] unless a liquid or vapor quenching is applied after deposition.[39] The spectra of ε_2 for the Cu−Ag alloys (Figure 3h) show two distinct absorption edges in the visible range, at 300 and 530 nm, indicating the independent contribution from both metals.[39] For this system, the *d*-bands from the pure metals slightly overlap, and the electron density of states from each metal contributes separately to the dielectric function of Cu−Ag alloys.[22] Our measurements show that both ε_1 and ε_2 can assume values higher and lower than what would be wrongly predicted by the composition-weighted linear combination, see Figures S7−S9. The discrepancy between the simple linear combination of the optical response of the combined pure metals and the actual quantities obtained for ε_1 differ by >50% for Au_xCu_{1-x} and >40% for Cu_xAg_{1-x}, and for ε_2 it can differ by more than 15% (see Figures S7−S9).

The quality factor of the surface plasmon polariton of the alloys, defined as $Q_{SPP} = (\varepsilon_1^2/\varepsilon_2) \times 10^{-3}$,[20] was calculated from the measurements of ε, and we found that certain compositions ($Ag_{0.5}Au_{0.5}$, $Au_{0.1}Cu_{0.9}$, and $Cu_{0.1}Ag_{0.9}$) present higher values of Q_{SPP} than the respective pure metals (see Figures 3c,f,i, S10, and S11). For instance, the disordered mixture of $Ag_{0.5}Au_{0.5}$ showed the largest values of Q_{SPP} for wavelength >600 nm, with maximum value at ∼830 nm, suggesting that a higher electron mean free path in the mixture of Ag and Au can provide a less absorptive material for NIR applications. Note that in all cases higher wavelength-dependent values of Q_{SPP} could be obtained by optimizing the deposition rate of each metal;[31] nonetheless, the trend of the relative improvement in Q_{SPP} as a function of the alloy composition should be the same, independent of the deposition rate used. Similarly, selected compositions of the binary-alloyed films exhibit higher propagation length of surface plasmon polariton than the pure metals (see Figure S11). To validate the ellispometry model, we determined scatter bands for transmission taking into account a film thickness variation of ±3 nm (see Figure S12), finding that the originally obtained thicknesses are the best match to our experimental data.

The SPP angle-dependent reflection spectra for all samples were measured using the Kretschmann configuration,[40] using a 637 nm diode laser *p*-polarized with 3.6 mW. The metal alloy thin film was placed on a rotational stage with step size of 0.1° and attached to an equilateral CaF_2 prism with n_{prism} = 1.433 using an index matching fluid for effective light coupling (see Methods for experimental details). As shown in Figure 4, in all cases (under identical experimental conditions), a well-defined minimum of the reflected laser power was observed, confirming the excitation of surface plasmons. Figure 4a,b displays the measured and calculated reflection spectra for the Ag−Au alloys, where the $Ag_{0.5}Au_{0.5}$ thin film presents a fairly shallow dip. Here, the small discrepancy between the measured and calculated angle is primarily due to (i) the uncertainty of the initial angle on the rotation stage (<0.1°), (ii) the presence of contaminants at the film surface, and (iii) the temperature variation of the sample during the SPP measurements.[40−42] The minimum reflection

DOI: 10.1021/acsphotonics.5b00586
ACS Photonics 2016, 3, 507−513

point for the Au_xCu_{1-x} alloys varies nonlinearly and nonmonotonically as a function of the composition (see Figure 4c,d), in agreement with the ellipsometry measurements presented in Figure 3c. According to Figure 4e,f, despite the fact that the Cu-based alloys are formed by ~50 nm grains (see Figure S3 for AFM images) and that an extremely thin layer of Cu_2O is present (Figure S13), the SPP coupling angle is very well-defined.

We find excellent agreement between the values of ε_1 measured by SPP coupling measurements and those obtained from ellipsometry, see Figure 5a−c, two independent techniques. The real part of the dielectric function for each pure metal and the alloys (ε_1^m) were calculated using the following equation:[40]

$$(n_{\text{prism}} \times \sin\,\theta_{\text{SPP}})^2 = \frac{\varepsilon_1^m \times \varepsilon_1^{\text{air}}}{\varepsilon_1^m + \varepsilon_1^{\text{air}}}$$

where n_{prism} is the refractive index of the prism, θ_{SPP} is the angle of minimum reflection in the SPP measurement, and $\varepsilon_1^{\text{air}}$ (=1) is the real part of the dielectric function for air. From the measured value of the internal angle corresponding to the minimum of the reflected power and the refractive index of the prism, we calculated ε_1 at 637 nm, and compared the results with the independent values obtained by the ellipsometry measurements on the same region of the samples. As confirmed by the latter, both Ag−Au and Au−Cu alloys only have one absorption edge over the visible range of the spectrum. As a result, the *d* bands strongly overlap in these systems, and the value of ε_1 varies as a function of the composition and the amount of overlap. For Au_xCu_{1-x}, ε_1 decays almost monotonically as a function of x (see Figure 5b). The disordered AuCu and $AuCu_3$ alloys lead to constant values of ε_1 (for $0.48 < x < 0.52$ and $0.71 < x < 0.77$), corroborating Rivory's hypothesis that ordering/disordering can strongly affect the optical properties of these binary mixtures.[22] The dielectric function of very thin films is extremely sensitive to the film overall thickness, the grains' size and the density of interfaces. As a result of the metal deposition conditions implemented, one can obtain thin films with a strong porous character and a high density of interfaces, which can result in additional light scattering centers and enhanced light absorption by the thin film.[38] In these situations, the effect of ordering on the dielectric function is indeed negligible, as the characteristic atomic disordering causes a "flattening" of the double peak usually observed in ordered Au−Cu (at ~330 nm for $Au_{0.5}Cu_{0.5}$, according to ref 22). The optical response of the Cu−Ag system is substantially different: the alloys do not form a solid solution and the value of ε_1 decreases almost linearly from pure Cu to pure Ag,[22,39] see Figure 5c. In this mixture, the *d* bands do not overlap strongly.

Here we show evidence that the chemical composition of noble metal alloys can affect the dielectric function of the material in nontrivial ways, modifying both the strength of the polarization induced by an external electric field and the losses in the material due to absorption. Finding the precise physical origin of the nonmonotonic behavior of ε_1 for the alloys would require determining their band diagram and the density of states by X-ray photoelectron spectroscopy measurements as a function of their composition, which is beyond the scope of this work. Nevertheless, we have shown that depending on the wavelength range of interest, the alloying of noble metals yields materials with controlled optical response, such as enhanced surface plasmon propagation length or minimized optical loss.

In conclusion, we have shown the correlation between the chemical composition of noble metal alloyed thin-films and their respective dielectric functions, which can be tailored by tuning the composition fraction between the two metals. Our ellipsometry and SPP excitation measurements are in excellent agreement, demonstrating the validity of the ellipsometry analysis. Moreover, we have shown that for the deposition conditions implemented here the Q_{SPP} of some alloyed mixtures is higher than the respective pure metals, allowing for the rational design of metallic nanostructures with a high control of their optical response in the visible range of the spectrum. Our approach to fabricate a new class of metallic materials with optical response on-demand can be applied to metasurfaces and metamaterials, which commonly requires low optical loss materials, hot carrier devices, whose performance is very sensitive to the light absorption within the active layer, and other optical and optoelectronic devices.

METHODS

Sample Fabrication. All metal-alloyed thin films were fabricated by the cosputtering deposition of single metals, at room temperature, with deposition rates between 2.0 and 5.0 Å/s, onto 4 × 6 in^2 glass slides. The glass slides were cleaned with acetone, isopropanol, and DI water, and then dried with N_2, prior the physical deposition. The pure metal sources (with purity > 99.99%) were placed 180° from each other, allowing for a linear gradient in composition for each alloyed sample (see Figure S1 and Table S1 in the SI).

Transmission and Reflection Measurements. The transmission and reflection measurements were performed using a variable-angle spectroscopic ellipsometer with a white-light source over a wavelength range of 200−1000 nm. Incident angles (with respect to normal incidence) of 60, 65, and 70° were used for reflection and 0° for transmission measurements. The ellipsometry data were analyzed using a B-spline model to determine the dielectric function for each pure metal and for the alloys, by assuming a two-layer vacuum-metal model to extract the dielectric function of each pure metal and each alloy.

Modeling the Dielectric Function. The dielectric function of each pure metal and the corresponding binary alloys was parametrized by B-spline functions $S(x)$, defined as[35]

$$S(x) = \sum_{i=1}^{n} c_i B_i^k(x)$$

where c_i is the B-spline coefficient and $B_i^k(x)$ is a B-spline basis function defined as

$$B_i^0(x) = \begin{cases} 1 & t_i \le x < t_{i+1} \\ 0 & \text{otherwise} \end{cases}$$

$$B_i^k(x) = \left(\frac{x - t_i}{t_{i+k} - t_i}\right) B_i^{k-1}(x) + \left(\frac{t_{i+k+1} - x}{t_{i+k+1} - t_{i+1}}\right) B_i^{k-1}(x)$$

where t_i is the perpendicular distance of the knot (where each polynomial segment in the curve is connected) from the y axis, and k is the degree of the B-spline. The Kramers−Kronig (K−K) relation was enforced during fitting to ensure the physical meaning of the results, as the imaginary part of the dielectric function ε_2 is parametrized by the B-spline curve as a function of wavelength λ as

$$\varepsilon_2(\lambda) = \sum_{i=1}^{n} c_i B_i^k(\lambda)$$

DOI: 10.1021/acsphotonics.5b00586
ACS Photonics 2016, 3, 507−513

Then, ε_1 was calculated using the Kramers−Kronig relation. Therefore, each reflection measurement was appended to the corresponding transmission spectrum and was fitted using the Kramers−Kronig enforced B-spline model simultaneously. Roughness was neglected during fitting of the measured data due to the minimal root-mean-squared (RMS) surface roughness of the thin films (<1.7 nm), as determined by AFM. In all cases, the root mean square error (RMSE) of the fits was <4.3 (see Supporting Information for more details about RMSE), and the thickness of the film was also a variable (see Supporting Information for all measured values). For Cu-rich alloys, the thin layer of oxide was neglected in the modeling, as it was found that the thickness of the oxide layer is negligible (<0.55 nm) by considering this extra oxide layer using our model (see Figure S9).[31]

Surface Plasmon Polariton (SPP) Coupling Experiments. The SPP measurements were performed using the Kretschmann geometry,[40] using a 637 nm diode laser with 3.6 mW incident power. A half-wave plate was used to select *p*-polarized light. The metal alloy thin film was attached to an equilateral CaF_2 prism with n_{prism} = 1.433 using an index-matching fluid. The sample was placed on a rotational stage that allowed us to change the angle of incidence, and the reflected light was detected using a silicon photodiode. The power of the reflected light was recorded at each external angle with a step size of 0.1°. The internal angle was calculated from the external one by considering the equilateral geometric shape and the dielectric function of the prism. The internal angle, corresponding to the reflection power minimum, was designated as θ_{SPP}. The following equation was used to calculate the real part of the dielectric function for each pure metal and the alloys (ε_1^m):[40]

$$(n_{prism} \times \sin\,\theta_{SPP})^2 = \frac{\varepsilon_1^m}{\varepsilon_1^m + 1}$$

Transmission and SPP Calculations. The calculated transmission spectra and SPP spectra (R_{SPP}) were obtained using the equations below:[1]

$$\text{transmission} = \frac{T_{012,p} + T_{012,s}}{2}$$

$$T_{012,p} = \frac{t_{01,p}t_{12,p}\,\exp(-i\beta)}{1 + r_{01,p}r_{12,p}\,\exp(-i\beta)}$$

$$T_{012,s} = \frac{t_{01,s}t_{12,s}\,\exp(-i\beta)}{1 + r_{01,s}r_{12,s}\,\exp(-i\beta)}$$

$$R_{SPP} = \frac{r_{01,p} + r_{12,p}\,\exp(-i2\beta)}{1 + r_{01,p}r_{12,p}\,\exp(-i2\beta)}$$

where the transmission coefficient for p- ($t_{jk,p}$) and s-polarized ($t_{jk,s}$) light are defined as

$$t_{jk,p} = \frac{2N_j\,\cos\theta_j}{N_k\,\cos\theta_j + N_j\,\cos\theta_k}$$

$$\text{and } t_{jk,s} = \frac{2N_j\,\cos\theta_j}{N_j\,\cos\theta_j + N_k\,\cos\theta_k}$$

and the reflection coefficients for p- ($r_{jk,p}$) and s-polarized ($r_{jk,s}$) light are defined as

$$r_{jk,p} = \frac{N_k\,\cos\theta_j - N_j\,\cos\theta_k}{N_k\,\cos\theta_j + N_j\,\cos\theta_k}$$

$$\text{and } r_{jk,s} = \frac{N_j\,\cos\theta_j - N_k\,\cos\theta_k}{N_j\,\cos\theta_j + N_k\,\cos\theta_k}$$

where j, k = 0, 1, 2.

And the phase variation of the light is

$$\beta = \frac{2\pi d}{\lambda}(N_1^2 - N_0^2\,\sin^2\,\theta_0)^{1/2}$$

where d is the thickness of the film, as determined by ellipsometry (see Tables S2−4 for values).

In the transmission calculations, 0 stands for air, 1 for the metal thin-film layer, and 2 for the glass substrate. In the SPP calculations, 0 refers to the prism, 1 to the metal thin-film layer, and 2 to air, N is the experimentally determined complex refractive index of each layer, and θ is the incidence angle of light (with wavelength λ) with respect to the normal direction.

■ ASSOCIATED CONTENT

Supporting Information

The Supporting Information is available free of charge on the ACS Publications website at DOI: 10.1021/acsphotonics.5b00586.

Scanning electron microscopy, atomic force microscopy, X-ray diffraction, transmission electron microscopy, energy-dispersive X-ray spectroscopy, ellipsometry data, dielectric function of alloyed thin-films from experimental data and calculated results using linear combination of pure metals, SPP propagation length and tables of optical properties for the pure metal and alloyed films, quality factors for pure metal thin films (PDF).

■ AUTHOR INFORMATION

Corresponding Author

*E-mail: mleite@umd.edu.

Notes

The authors declare no competing financial interest.

■ ACKNOWLEDGMENTS

We gratefully acknowledge fruitful discussions with J. N. Munday, M. R. Dias, and J. Murray, the critical reading of D. Serrano, the technical assistance from G. Henein and J. Schumacher at the CNST/NIST Nanofab, P. Z. Zavalij at the X-ray Crystallographic Center, V. Ray and S. Liou at the AIMLab, and the Maryland NanoCenter, UMD. Research performed in part using the infrastructure at the NIST Center for Nanoscale Science and Technology. This material is based upon work supported by the National Science Foundation under Grant No. HRD1008117 and by the UMD ADVANCE program. The authors thank the financial support from the Minta Martin Award at the Clark School of Engineering and the University of Maryland 2015 Graduate School's Summer Research Fellowship program.

■ REFERENCES

(1) Maier, S. A. *Plasmonics: Fundamentals and Applications*; Springer, 2007.

(2) Kats, M. A.; Blanchard, R.; Genevet, P.; Capasso, F. Nanometre optical coatings based on strong interference effects in highly absorbing media. *Nat. Mater.* **2012**, *12*, 20−24.

DOI: 10.1021/acsphotonics.5b00586
ACS Photonics 2016, 3, 507−513

(3) Kildishev, A. V.; Boltasseva, A.; Shalaev, V. M. Planar photonics with metasurfaces. *Science* **2013**, *339*, 1289.
(4) Park, J.; Kang, J.-H.; Vasudev, A. P.; Schoen, D. T.; Kim, H.; Hasman, E.; Brongersma, M. L. Omnidirectional Near-Unity Absorption in an Ultrathin Planar Semiconductor Layer on a Metal Substrate. *ACS Photonics* **2014**, *1*, 812−821.
(5) Zheng, B. Y.; Wang, Y.; Nordlander, P.; Halas, N. J. Color-Selective and CMOS-Compatible Photodetection Based on Aluminum Plasmonics. *Adv. Mater.* **2014**, *26*, 6318−6323.
(6) Knight, M. W.; Sobhani, H.; Nordlander, P.; Halas, N. J. Photodetection with active optical antennas. *Science* **2011**, *332*, 702−704.
(7) Hylton, N. P.; Li, X. F.; Giannini, V.; Lee, K. H.; Ekins-Daukes, N. J.; Loo, J.; Vercruysse, D.; Dorpe, P. V.; Sodabanlu, H.; Sugiyama, M.; Maier, S. A. Loss mitigation in plasmonic solar cells: aluminium nanoparticles for broadband photocurrent enhancements in GaAs photodiodes. *Sci. Rep.* **2013**, *3*, 2874.
(8) Catchpole, K.; Polman, A. Plasmonic solar cells. *Opt. Express* **2008**, *16*, 21793−21800.
(9) Green, M.; Pillai, S. Harnessing plasmonics for solar cells. *Nat. Photonics* **2012**, *6*, 130.
(10) Landy, N. I.; Sajuyigbe, S.; Mock, J. J.; Smith, D. R.; Padilla, W. J. Perfect Metamaterial Absorber. *Phys. Rev. Lett.* **2008**, *100*, 207402.
(11) Naik, G. V.; Shalaev, V. M.; Boltasseva, A. Alternative plasmonic materials: beyond gold and silver. *Adv. Mater.* **2013**, *25*, 3264−94.
(12) Naik, G. V.; Saha, B.; Liu, J.; Saber, S. M.; Stach, E. A.; Irudayaraj, J. M. K.; Sands, T. D.; Shalaev, V. M.; Boltasseva, A. Epitaxial superlattices with titanium nitride as a plasmonic component for optical hyperbolic metamaterials. *Proc. Natl. Acad. Sci. U. S. A.* **2014**, *111*, 7546−7551.
(13) Soukoulis, C. M.; Koschny, T.; Tassin, P.; Shen, N.-H.; Dastmalchi, B. What is a good conductor for metamaterials or plasmonics. *Nanophotonics* **2015**, *4*, 69−74.
(14) Cortie, M.; Giddings, J.; Dowd, A. Optical properties and plasmon resonances of titanium nitride nanostructures. *Nanotechnology* **2010**, *21*, 115201.
(15) Stuart, H. R.; Hall, D. G. Absorption enhancement in silicon-on-insulator waveguides using metal island films. *Appl. Phys. Lett.* **1996**, *69*, 2327.
(16) Cortie, M. B.; McDonagh, A. M. Synthesis and Optical Properties of Hybrid and Alloy Plasmonic Nanoparticles. *Chem. Rev.* **2011**, *111*, 3713−3735.
(17) Cao, W.; Chang, Y.; Zhu, J.; Chen, S.; Oates, W. Thermodynamic modeling of the Cu−Ag−Au system using the cluster/site approximation. *Intermetallics* **2007**, *15*, 1438−1446.
(18) Link, S.; Wang, Z. L.; El-Sayed, M. A. Alloy Formation of Gold−Silver Nanoparticles and the Dependence of the Plasmon Absorption on Their Composition. *J. Phys. Chem. B* **1999**, *103*, 3529−3533.
(19) Motl, N. E.; Ewusi-Annan, E.; Sines, I. T.; Jensen, L.; Schaak, R. E. Au−Cu Alloy Nanoparticles with Tunable Compositions and Plasmonic Properties: Experimental Determination of Composition and Correlation with Theory. *J. Phys. Chem. C* **2010**, *114*, 19263−19269.
(20) Blaber, M. G.; Arnold, M. D.; Ford, M. J. A review of the optical properties of alloys and intermetallics for plasmonics. *J. Phys.: Condens. Matter* **2010**, *22*, 143201.
(21) Amram, D.; Rabkin, E. Core(Fe)−Shell(Au) Nanoparticles Obtained from Thin Fe/Au Bilayers Employing Surface Segregation. *ACS Nano* **2014**, *8*, 10687−10693.
(22) Rivory, J. Comparative study of the electronic structure of noble-metal-noble-metal alloys by optical spectroscopy. *Phys. Rev. B* **1977**, *15*, 3119−3135.
(23) Papaconstantopoulos, D. *Handbook of the Band Structure of Elemental Solids*; Plenum Press: New York, 1986.
(24) Gaudry, M.; Lermé, J.; Cottancin, E.; Pellarin, M.; Vialle, J.-L.; Broyer, M.; Prével, B.; Treilleux, M.; Mélinon, P. Optical properties of $(Au_xAg_{1-x})_n$ clusters embedded in alumina: evolution with size and stoichiometry. *Phys. Rev. B: Condens. Matter Mater. Phys.* **2001**, *64*, 085407.
(25) Palik, E. D. *Handbook of Optical Constants of Solids II*; Academic Press, 1991.
(26) Rioux, D.; Vallières, S.; Besner, S.; Muñoz, P.; Mazur, E.; Meunier, M. An Analytic Model for the Dielectric Function of Au, Ag, and their Alloys. *Adv. Opt. Mater.* **2014**, *2*, 176−182.
(27) Schulz, L. G. The Optical Constants of Silver, Gold, Copper, and Aluminum. I. The Absorption Coefficient k. *J. Opt. Soc. Am.* **1954**, *44*, 357−362.
(28) Cooper, B. R.; Ehrenreich, H.; Philipp, H. R. Optical Properties of Noble Metals. II. *Phys. Rev.* **1965**, *138*, 494−507.
(29) Palik, E. D. *Handbook of Optical Constants of Solids*; Academic Press, 1998; Vol. 3.
(30) Johnson, P. B.; Christy, R. W. Optical Constants of the Noble Metals. *Phys. Rev. B* **1972**, *6*, 4370−4379.
(31) McPeak, K. M.; Jayanti, S. V.; Kress, S. J. P.; Meyer, S.; Iotti, S.; Rossinelli, A.; Norris, D. J. Plasmonic Films Can Easily Be Better: Rules and Recipes. *ACS Photonics* **2015**, *2*, 326−333.
(32) Gu, D.; Zhang, C.; Wu, Y.-K.; Guo, L. J. Ultrasmooth and Thermally Stable Silver-Based Thin Films with Subnanometer Roughness by Aluminum Doping. *ACS Nano* **2014**, *8*, 10343−10351.
(33) Kossoy, A.; Merk, V.; Simakov, D.; Leosson, K.; Kéna-Cohen, S.; Maier, S. A. Gold Films: Optical and Structural Properties of Ultra-thin Gold Films. *Adv. Opt. Mater.* **2015**, *3*, 1−1.
(34) Tompkins, H. G.; Tasic, S.; Baker, J.; Convey, D. Spectroscopic ellipsometry measurements of thin metal films. *Surf. Interface Anal.* **2000**, *29*, 179−187.
(35) Johs, B.; Hale, J. S. Dielectric function representation by B-splines. *Phys. Status Solidi A* **2008**, *205*, 715−719.
(36) Lubarda, V. On the effective lattice parameter of binary alloys. *Mech. Mater.* **2003**, *35*, 53−68.
(37) Wei, S.-H.; Mbaye, A.; Ferreira, L.; Zunger, A. First-principles calculations of the phase diagrams of noble metals: Cu-Au, Cu-Ag, and Ag-Au. *Phys. Rev. B: Condens. Matter Mater. Phys.* **1987**, *36*, 4163.
(38) De Silva, K.; Gentle, A.; Arnold, M.; Keast, V.; Cortie, M. Dielectric function and its predicted effect on localized plasmon resonances of equiatomic Au−Cu. *J. Phys. D: Appl. Phys.* **2015**, *48*, 215304.
(39) Song, J.; Li, H.; Li, J.; Wang, S.; Zhou, S. Fabrication and optical properties of metastable Cu−Ag alloys. *Appl. Opt.* **2002**, *41*, 5413−5416.
(40) Pluchery, O.; Vayron, R.; Van, K.-M. Laboratory experiments for exploring the surface plasmon resonance. *Eur. J. Phys.* **2011**, *32*, 585.
(41) Matsubara, K.; Kawata, S.; Minami, S. Optical chemical sensor based on surface plasmon measurement. *Appl. Opt.* **1988**, *27*, 1160−1163.
(42) Novotny, L.; Hecht, B. *Principles of Nano-Optics*; Cambridge University Press, 2011.

NOTE ADDED AFTER ASAP PUBLICATION

An erroneous Supporting Information file was published on February 29, 2016. The corrected version was reposted on March 22, 2016.

DOI: 10.1021/acsphotonics.5b00586
ACS Photonics 2016, 3, 507−513